SGER: Resonant Microsensor Based on Decoupled Sensing Scheme for Liquid-Phase Biochemical Sensing

Final Report: Project Activities

L.A. Beardslee, O. Brand

School of Electrical and Computer Engineering
Georgia Institute of Technology, Atlanta, GA 30332

Abstract: A new sensor concept potentially leading to high-resolution liquid-phase biochemical sensors was designed and fabricated. Preliminary tests on a fabricated device were performed in air. Based on these results, process modifications were implemented and a packaging process ensuring vacuum encapsulation of the resonant microsensor was developed. Overall, as part of the 15-months project, a mask layout for the novel sensor concept was developed, an entirely new fabrication process was designed, tested and implemented. In addition, resonator dies were initially tested using a transimpedance amplifier connected to a network analyzer.

1. Introduction

Several different approaches have been investigated for detection of biochemical analytes in aqueous media. Of particular interest is the development of a single chip or a single package solution where both the sensor structure and the circuitry to operate it can be batch fabricated in the same process sequence. This saves time and cost, allowing the sensors to be deployed in environmental monitoring or for disposable biomedical applications [1]. Two promising sensor platforms for this purpose are capacitive devices and gravimetric sensors. Capacitive and other electrochemical sensors are widely used, but typically require complex external driving circuits that limit where the sensors can be deployed [2]. Resonant gravimetric sensors can be readily miniaturized and integrated with circuitry, but suffer from large damping and thus reduced signal to noise ratio when operated in a liquid [3]. In contrast, in air or vacuum, MEMS resonators can provide high signal to noise ratio and are being investigated to replace quartz resonators in oscillator applications [4].

The goal of this project was to investigate a scheme for liquid-phase biochemical sensing, which combines the advantages of MEMS resonators and capacitive sensors, i.e. high resolution, high sensitivity and the ability to be miniaturized and integrated with CMOS (complimentary metal oxide semiconductor) circuitry. To do this the investigated structure uses the spring-softening effect in an electrostatically actuated beam as the transduction mechanism. As mentioned above, such a device is needed in liquid sensing applications for two main reasons: (1) operation of a gravimetric sensor in the liquid itself creates substantial damping, which raises the sensor limit of detection due to the decreased signal to noise ratio. Drying the device after liquid exposure has been proposed but requires washing, which would add additional steps and thus complexity to a system on a chip solution; (2) in case of harsh or corrosive environments, direct exposure of the resonator to the liquid can cause the device to fail. Isolating the delicate resonator structure from the environment would thus lead to improvements in both resolution and reliability. In

order to isolate the resonator from the fluid containing the analyte, a concept is investigated where the sensing element is the capacitance of the fluid channel. Changes in the dielectric constant inside the fluid channel due to analyte binding cause a change in the channel's capacitance which is read out using a MEMS resonator. The resonator essentially acts as an analog to digital converter, converting the capacitance change to a frequency change, which can be tracked using a digital counter.

2. Device Concept

The basic device concept is shown in Fig. 1 and consists of a clamped-free or clamped-clamped beam resonator with two sets of electrodes. These electrodes are placed on each side of a microfluidic channel; thus, the sample fluid is in contact with the (functionalized) electrodes but not with the resonator itself. The beam is fixed at a negative DC voltage and the two outer electrodes are placed at a positive DC potential. The electrodes between the air gaps and the fluid channel are at a floating potential, which is affected by the (bio)chemical interaction of the sample fluid with the functionalized electrodes.

The actual device operation is based on the well-known electrostatic spring-softening effect [5]. Thereby, the spring softening is used to couple the change in fluid channel capacitance to resonator frequency. The spring softening effect is a nonlinear phenomenon arising from the capacitance change that occurs when an electrostatic resonator gets close to the transduction electrode during device operation. An applied DC voltage on the transduction electrodes will cause the resonant frequency of the resonator to drop as the bias is increased. This can be utilized as a transduction mechanism for a sensor if a method can be found to couple this change in DC bias to a change in the analyte concentration of interest. In the case of this investigation, a capacitive divider is used so that the DC voltage on an intermediate electrode, between the fluid and the resonator air gap, changes with the concentration of analyte. Analyte binding within the fluid channel effects the capacitance of the fluid channel, thus the voltage on the intermediate electrode between the fluid channel and the second capacitor in the divider (the second capacitor is the resonator air gap), will change.

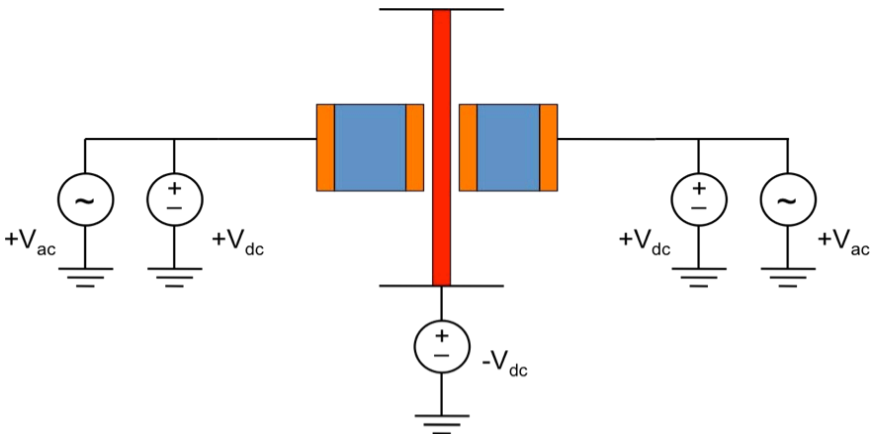

Figure 1: *Proposed sensor structure with electrostatic beam resonator (red), static electrodes (orange) and fluid channels (blue).*

The electrostatics of the device shown in Fig. 1 can be modeled as two capacitors in series, whereby the bio(chemical) sensing modifies the potential of the floating electrode either through a change of the dielectric properties inside the fluid channel or a surface charge on the (functionalized) electrodes. This modulates the DC voltage drop across the air region, which controls the spring softening. The two capacitors form a capacitive voltage divider, and the voltage on the floating electrodes is given by

$$V = V_{dc} \frac{\varepsilon_f g - \varepsilon_a d_f}{\varepsilon_f g + \varepsilon_a d_f} \tag{1}$$

where V_{dc} is the voltage on the fixed electrodes, ε_f is the dielectric constant of the fluid, ε_a is the dielectric constant of the air, g is the width of the air gap and d_f is the width of the fluid channel. Thus, changing the dielectric constant of the fluid will change the voltage on the floating electrode.

For a clamped-clamped beam the magnitude of the spring-softening effect can be found by differentiating the net electrostatic force, resulting in an electrostatic spring constant:

$$k_e = \left[\frac{V_1^2 \varepsilon_a A}{g^3}\right] + \left[\frac{V_2^2 \varepsilon_a A}{g^3}\right] \tag{2}$$

with V_1 and V_2 being the voltages on the floating conductors, and A the area of the floating conductors. Once the electrostatic spring constant k_e has been determined, the relative shift of the resonance frequency of the beam is given by

$$\frac{\Delta f}{f} = \sqrt{1 - \frac{k_e}{k_m}} \tag{3}$$

with the mechanical spring constant k_m of the clamped-clamped beam. Using the above equations, the relative frequency change was estimated for a 350 µm long, 4.5 µm wide and 8µm thick silicon beam (a 50 µm section in the center of the beam is 13 µm wide), a floating electrode area of 50 µm by 8 µm, a 0.8 µm air gap and a 40 µm wide fluid channel. Using V_{dc} = 15 V, a change of the dielectric constant in the fluid channel from 80 to 80.3 (i.e., 0.375%) results in a frequency change of 43 Hz at a base frequency of approx. 300 kHz. The hand calculations have been confirmed using finite element simulations performed with *CoventorWare*, which predicts a frequency change of 33 Hz for the above dimensions.

If the sensor is packaged using an on-chip vacuum packaging scheme, the resonator itself could be operated in vacuum, this would allow a very high Q to be obtained from the resonator, giving an excellent short-term frequency stability and thus signal to noise ratio. This would lead to high sensor resolution.

Figure 2 shows the CAD layout of an actually implemented design with the beam resonator, the three electrodes with the intermediate electrode being the floating electrode and the fluidic microchannel. The connections shown were used to initially characterize the sensor structure.

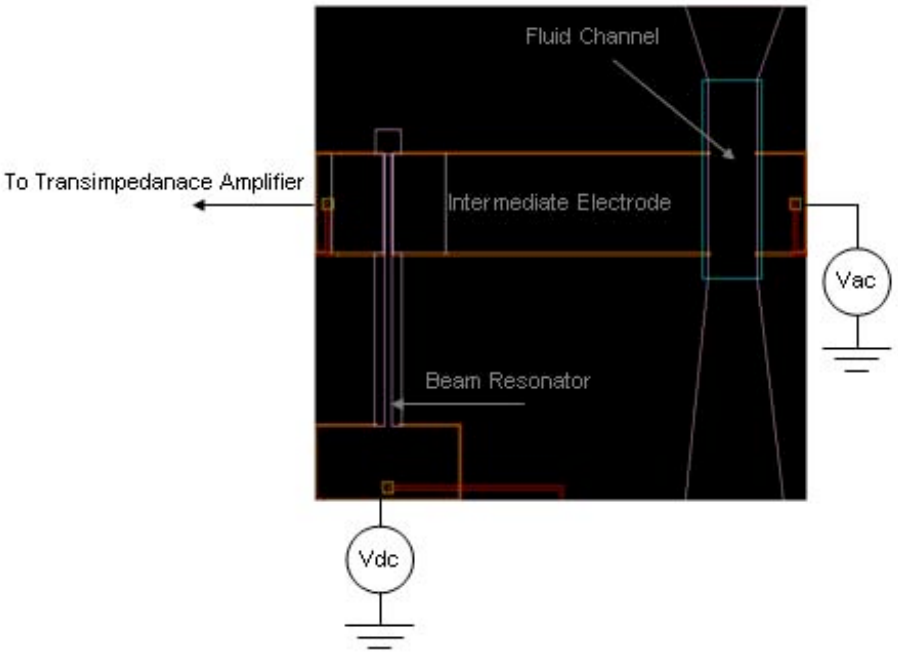

Figure 2: *The wiring of a beam resonator shown on a CAD layout, the electrode labeled intermediate electrode is the node that changes DC voltage in response to a dielectric constant change within the fluid channel.*

3. Device and Die Layout

Different variations of the structure shown in Fig. 2 above were designed using Cadence. In total, 42 unique devices were designed, and a total of 330 dies were created in the 100-mm mask layout. In terms of device operation, the resonators were designed for fabrication on SOI (silicon on insulator) wafers with a degenerately doped device layer. To prevent shorting between the electrodes, a silicon nitride isolation was used around the electrodes. Patterned metal lines were drawn to connect the electrodes on each device to bond pads, which were used for testing. The die layout contains 4 different resonators, which share fluid channels. A through wafer hole is used for microfluidic packaging: by placing the die in a manifold and sealing the fluid channel from the top using a wafer bonding technique, fluid can be injected up through the holes, into the fluid channel and exit through the second set of holes on the opposite end of the die (See Fig. 4). The manifold can easily be fabricated using stereolithography. A variety of resonator shapes were incorporated into the layout, including clamped-clamped beams, clamped-free beams and also tuning forks (See Figs. 2 and 3).

In an effort to reduce noise, and also lower the voltages needed for actuation, the resonators were designed so that they could be fabricated with submicron transduction gaps. In addition, several variations on the same device were drawn, including: having one or two fluid channels, having wider and narrower fluid channels, having wider and narrower conduction gaps and electrodes, different sizes of the same basic beam shapes, and different configurations allowing the resonators to be packaged by hand if needed. Finite element simulations (FEM) were used to find

beam shapes that had a range of resonance frequencies from 100 KHz to 1 MHz. FEM simulations were also used to find the best dimensions for the capacitive electrodes and fluid channels. Eventually, the devices need to be packaged using a hermetic process such as eutectic bonding, the device layout also leaves enough tolerances for this to be implemented.

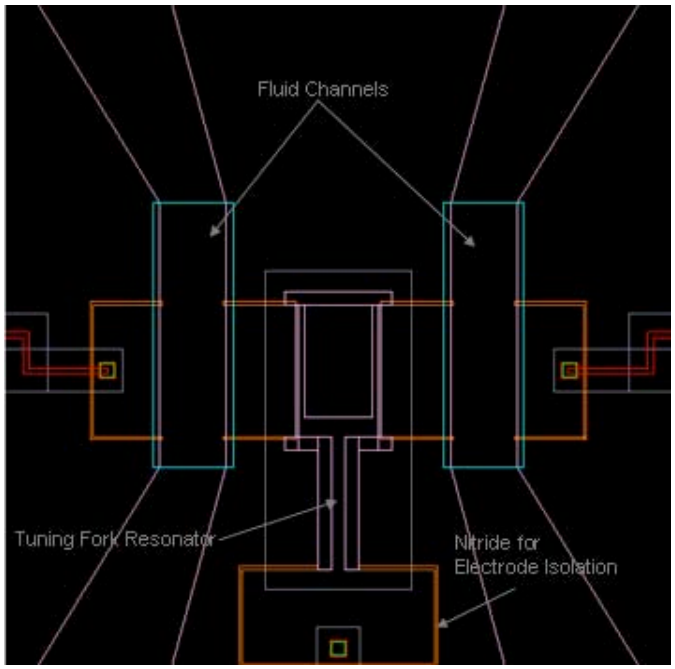

Figure 3: *Example of a tuning fork layout with labeled nitride-isolate electrodes as well as fluid channels and resonator.*

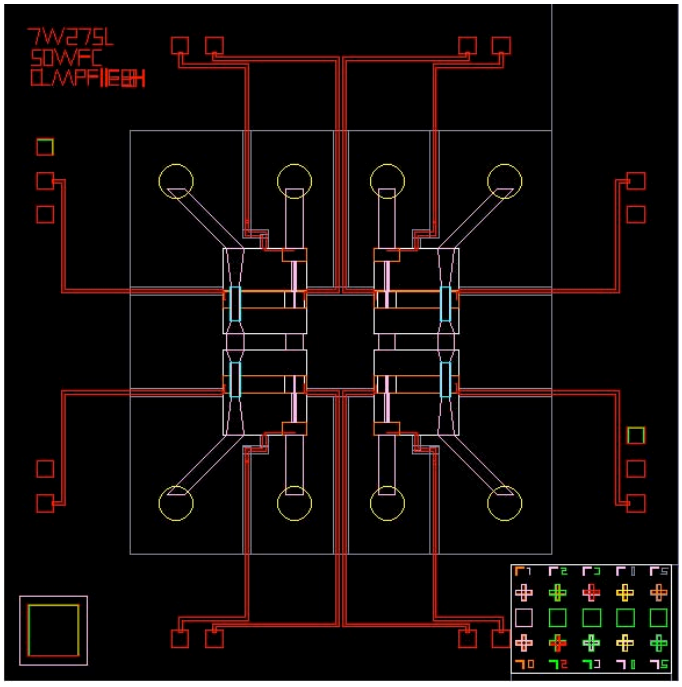

Figure 4: *Entire die layout for a die with 7μm wide and 275μm long cantilevers. The through holes for the fluid are shown in yellow and the metal lines are shown in red.*

4. Sensor Fabrication

To create working resonators from the layout, a new fabrication process was designed, tested, and implemented. The key parameters for successful device operation were (1) the nitride isolation to prevent electrode shorting and (2) the width of the transduction gaps. To create the isolation, trenches were first ICP-etched down to the BOX (buried oxide) layer of an SOI wafer and then backfilled with LPCVD nitride. It was found that the as-deposited nitride was too conductive to provide effective isolation, so in subsequent processing runs a thermal oxide was grown to aid the electrical isolation. The submicron transduction gaps were created using an oxidation process to narrow the gaps, similar to the process presented in [6]. Using a trench closure process based on oxidation precludes the need for expensive, non-CMOS compatible processes such as E-beam lithography. One note about the processing is that for a first trial of the packaging process using wafer bonding, the devices were bonded using a polymer bonding process, instead of a hermetic process. It was believed that the polymer bonding would be easier to implement. However, the initial results showed the polymer reflows and blocks the resonator operation; as a result, a bonding process based on eutectic bonding was subsequently developed and is described in Chapter 6. The entire initial process flow with schematic process cross-sections is summarized below. The process was implemented using fabrication tools available at Georgia Tech's Nanotechnology Research Center.

4.1. Process Sequence

The process is based on SOI wafers with a 10 μm thick degenerately doped p-type device layer, a 2μm thick BOX layer and a 500 μm thick p-type handle layer.

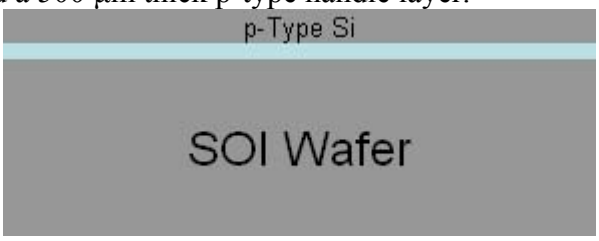

1. Pattern wafer with *Trench Isolation Etch* mask and ICP etch trenches into the silicon to isolate electrodes.

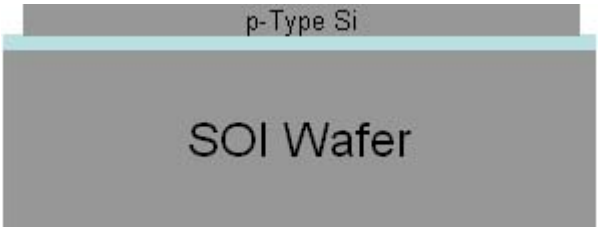

2. Grow 300 nm of thermal oxide (wet oxidation) to improve trench electrical isolation.
3. Backfill trenches with 1.5-2 μm of LPCVD nitride using Tystar Nitride Furnace 4.
4. Etch back nitride on surface until 400-600 nm remain using Plasma Therm ICP.
5. Strip nitride from wafer backside using the Plasma Therm ICP (doing this ensures that the etch mask for the fluidic holes is actually etched to the bare silicon on the SOI wafer backside.)
6. Deposit 2-2.5 μm of polysilicon using Tystar Poly Furnace 4.
7. Pattern wafer topside with *Resonator Definition* mask and ICP etch polysilicon.
8. Grow 1.7-2 μm of oxide in one of the Tystar Furnaces (wet oxidation).

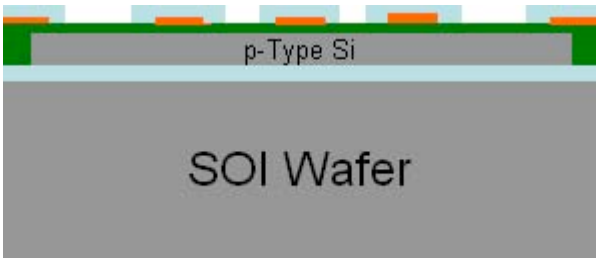

9. Etch nitride using the oxide layer as mask using the Plasma Therm ICP.

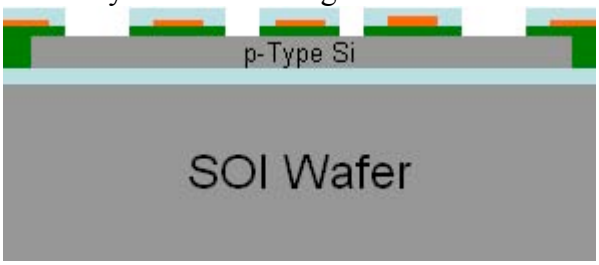

10. Strip thermal oxide with BOE.
11. Pattern wafer topside with *Packaging* mask.
12. Etch device layer using STS Pegasus; the packaging etch and device definition are both done during this step. (Even if eutectic bonding is not used, the packaging etch must be done to prevent metal line shorting by the polysilicon.)

13. Pattern topside with *Contact Opening* mask and etch nitride with the Plasma Therm ICP.
14. Deposit 4 µm of PECVD oxide on wafer backside using the STS PECVD; the SiO_2 etch mask is used for the through wafer etch of the microfluidic access holes.
15. Pattern backside with *Backside Port Etch* mask and etch oxide using the Plasma Therm ICP.
16. Clean wafer in Piranha etch for 10 min and perform 5 cycles in a quick dump rinser.
17. Coat wafer topside with negative resist and pattern with *Metal* mask.
18. Deposit 500 nm of gold on wafer in an e-beam evaporator and pattern gold using lift-off.*

19. Clean wafer thoroughly with Piranha etch and DI H_20.
20. Pattern wafer topside using 10-15 µm of SU-8 and *Packaging* mask.**
21. ICP etch through wafer from the backside using the Plasma Therm ICP.

22. Dice the wafer.
23. Release the devices individually in HF and check the release with an IR microscope.

24. Dice a borofloat quartz wafer to create squares.**
25. Bond the SOI wafer with devices to the quartz wafer in the Karl Suss bonder.**
26. Apply ALD TiO_2 passivation.**

* For initial experiments, gold was chosen as the metallization. Gold is extremely inert allowing for device release after dicing and also more thorough cleaning of the wafer with Piranha etch after metallization. Eventually, the process could be implemented using aluminum metallization.
** These steps were not implemented initially; towards the end of the project, a packaging process was developed, and wafers that integrate the sensor and the packaging process sequences are currently (beyond the NSF funding period) being processed at the NRC facility and will be tested subsequently.

4.2. Fabrication Results

Before the process above was implemented on SOI wafers, it was first tested to the extent possible on prime-grade silicon wafers. The SOI wafers that were used had degenerately doped p-type device layers and a 2 μm BOX layer.

Figs. 5, 6 and 7 show details of the fabricated devices, namely the sub-micrometer transduction gaps between the resonating beams and the floating electrodes and the nitride/oxide isolation between the electrodes. Fig. 8 shows a completed device with a clamped-clamped beam resonator, the microfluidic channel, the floating electrode, as well as the gold interconnections to the bond pads.

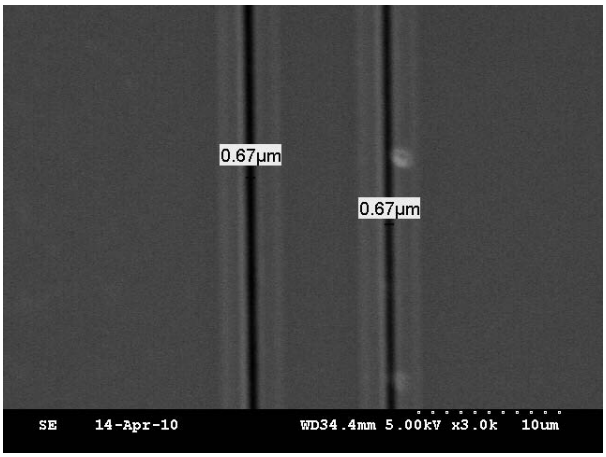

Figure 5: *Submicron transduction gaps between beam and floating electrodes with the widths shown on the figure.*

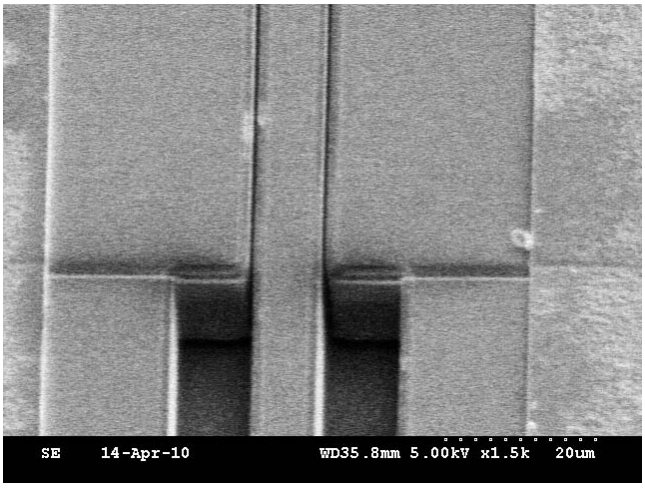

Figure 6: *Submicron transduction gaps shown on an etched resonator.*

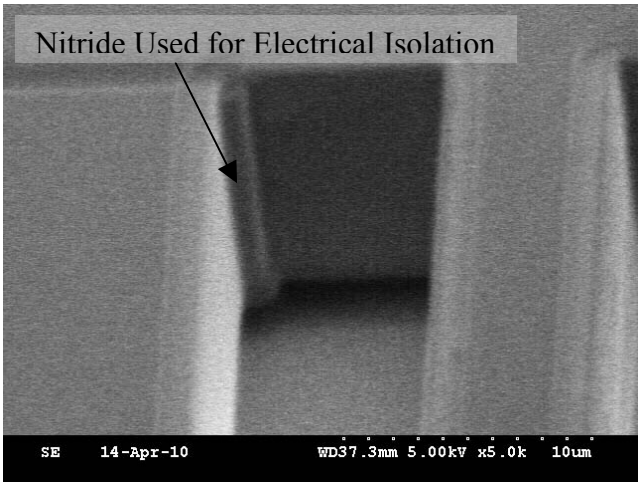

Figure 7: *Nitride trench isolation on a beam resonator. The nitride extends 2µm past the corner of the trench at the base of the resonator to ensure proper device insulation.*

The images presented above (Figs. 5-7) show that the fabrication process as implemented can achieve the above-mentioned goals of creating submicron transductions gaps with the designed structures. In addition, with the use of an oxide layer in addition to an LPCVD nitride layer for the trench isolation, the three electrodes on the device could be isolated from each other so that no resistance between them could be measured with a digital multi-meter.

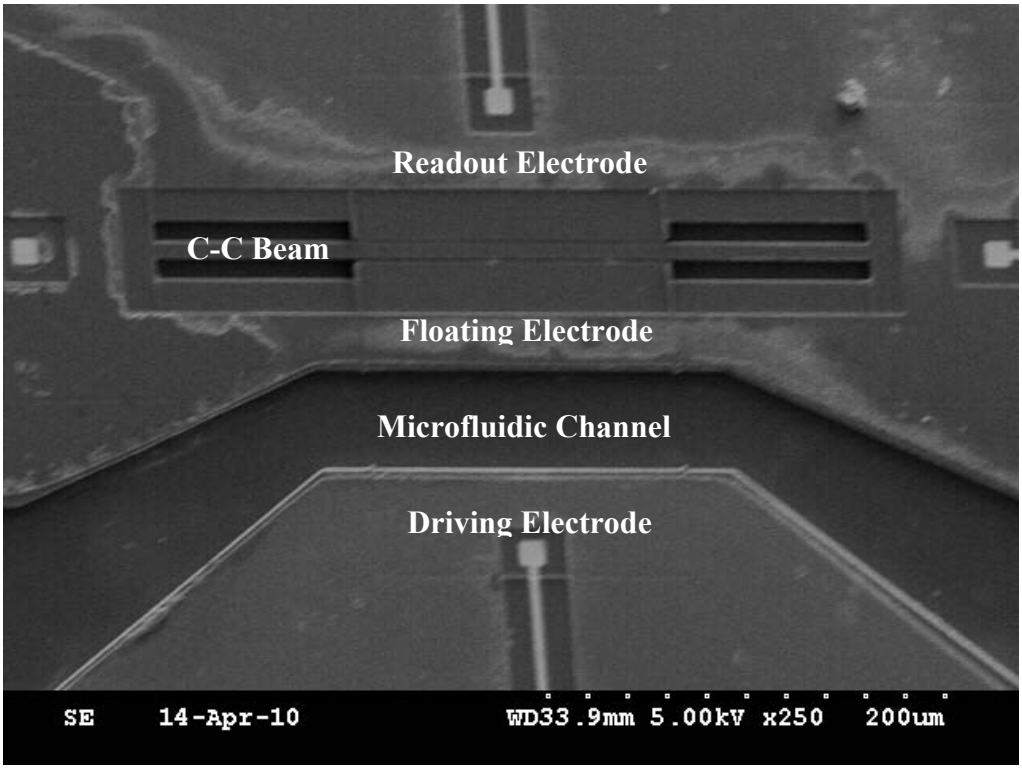

Figure 8: *Completely fabricated device based on clamped-clamped beam resonator with the fluid channel and all four electrical connections shown.*

5. Initial Resonator Testing

As indicated in Fig. 2, the devices were connected for testing to a transimpedance amplifier, which converts the resonator output current to a voltage that can then be read by a network analyzer. The phase and frequency response of a 7 μm wide, 275 μm long and 10 μm thick cantilever with 2 μm transduction gaps are shown in Fig. 9. The presented measurement has the crosstalk between the input and output signals been removed using MATLAB. The simulated resonance frequency for the tested device is 126.6 kHz with a silicon density of 2330 kg/m^3, a Young's modulus of 167 GPa, and a Poisson ratio of 0.07. The simulated and measured responses are similar, with the measured transfer characteristic showing a frequency of 129.9 kHz. The signal-to-noise ratio is rather small, stemming partly from the fact that the fluid channel was in this experiment not filled with water but with air, resulting in a substantially lower coupling capacitance. Moreover, squeezed film damping by the surrounding air reduces the Q-factor of the resonator to 6-7. Vacuum encapsulation of the resonator, which is currently

under development, is expected to strongly improve the Q-factor. The measurement shown in Fig. 9 was performed using a 15 V DC bias applied to the beam.

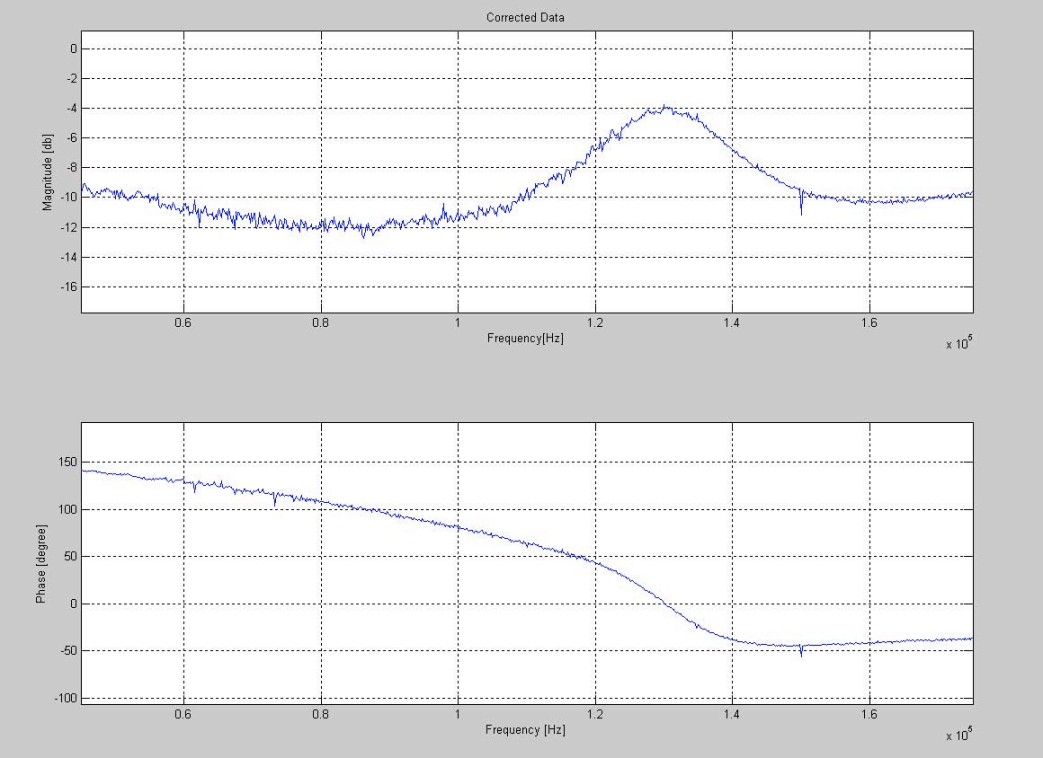

Figure 9: *Frequency response of a 7 µm wide, 275 µm long, and 10 µm thick clamped-free beam device.*

6. Sensor Packaging

A prerequisite for reliable liquid-phase testing of the proposed sensor structure is a packaging method that will allow for fluid to be injected into the proper area of the die while at the same time vacuum packaging the resonator. Originally, it was thought that a quick solution to allow for some basic testing would be a bonding process using SU8 as an adhesive to attach the cap wafer to the device wafer. After initial tests, this strategy was found to be problematic because during SU8 bonding the SU8 can deform and even flow. With the layout tolerances on the masks, even a modest amount of flow from the SU8 can cover the resonators rendering them useless. In light of the problems with the SU8 bonding, it was decided that a better strategy would be to go ahead and develop a gold-silicon eutectic bonding process (see Fig. 10).

The developed process is as follows: (1) approximately 600 nm of gold is DC sputtered onto a borofloat wafer using chromium as an adhesion layer, (2) the gold is patterned with negative tone resist and subsequently wet-etched using gold etchant, (3) the bonding wafer and the device wafer are aligned by hand under a microscope, (4) bonding is performed in Karl Suss SB8 bonder at 430˚C, with 2000 torr of pressure applied to the wafers for 150 minutes, the bonding process is performed under vacuum. After bonding, the borofloat wafer is diced almost all the

way through, so that the glass covering the bond pads can be split off. During processing of an actual device wafer, the bonding will be performed at the end of the process after resonator release in HF.

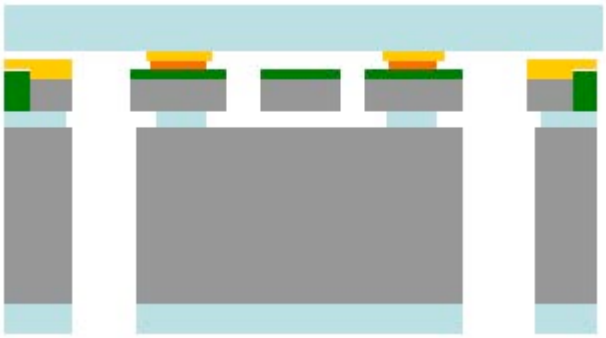

Figure 10: Proposed bonding process, the gold deposited on a borofloat wafer is eutectically bonded to the polysilicon (shown in orange) that is left after patterning with the packaging mask. Although not shown in this cross section, the bonding creates fluid channels that are isolated from both the electrical contacts and also the resonator itself.

For process characterization, the above bonding process was performed on a prime wafer that had polysilicon bonding structures patterned using the packaging mask deposited on top of silicon nitride. Initially, a process was tested where dicing streets were cut into the surface of the borofloat wafer before bonding. This process was unsuccessful, most likely because the dicing before bonding can leave ridges on the wafer surface and also dicing can leave particulates on the wafer. In the second attempt, both wafers to be bonded were thoroughly cleaned with Pirhana, and the bonding was performed before any dicing of the borofloat wafer. This process created a successful bond between the borofloat wafer and the test wafer coated with polysilicon (Figs. 11 and 12). After successful testing of the eutectic bonding process, the next step is the implementation of the process on an actual SOI device wafer in an attempt to release resonators that can be tested as liquid phase sensors.

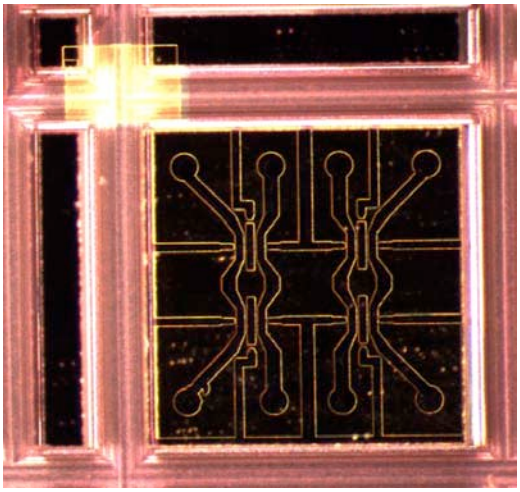

Figure 11: A bonded structure on the test wafer after the borofloat wafer was diced.

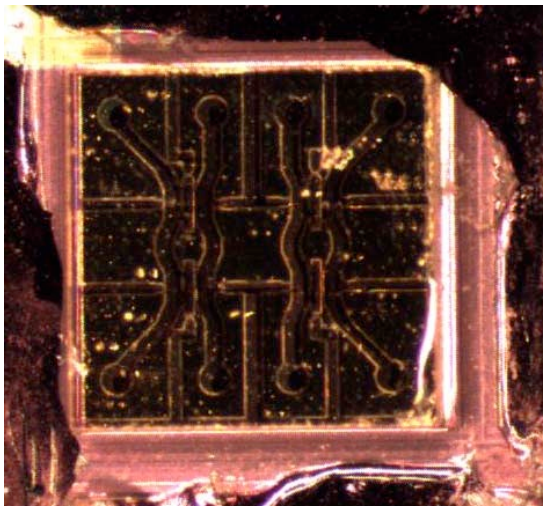

Figure 12: Bonded structure on the test wafer after the excess glass is broken away from the edges. On an actual device wafer, the silicon device wafer would be diced before this step (a cut would be made in the correct location through both the silicon device wafer and the borofloat wafer bonded to its surface; this is expected to facilitate access to the bonding pads).

7. Conclusions and Outlook

In conclusion, first devices for liquid-phase biochemical sensing based on a new decoupled sensing scheme were simulated, designed, and fabricated. Preliminary testing data (Fig. 9) for the fabricated devices show a resonant behavior at the expected frequencies, indicating that the proposed sensing structure functions as designed. Furthermore, a packaging process based on eutectic gold-silicon bonding was developed, which will enable vacuum encapsulation of the resonant microstructure and liquid-phase testing of the sensing device.

Since the NSF funding period has ended (July 31, 2010), we have started processing a sensor wafer based on the consolidated process sequence that now also incorporates the device packaging. It was our hope that by the due date of this final report, we would have completed devices available and first devices characterized. However, due to equipment down times, the wafer is not fully processed yet. We, however, expect device testing to be completed within the next 6 month, with the results hopefully being the foundation for a subsequent research proposal. Moreover, several publications stemming from the work are planned.

8. References

1. Brand, O. *Proceedings of the IEEE.* **2006**, 94, 1160-1176.
2. C. Berggren, G. Johansson, *Analytical Chemistry*, **1997**, 69, 3651-3657.
3. Vancura, C.; Li, Y.; Lichtenberg, J.; Kirstein, K. U.; Hierlemann, A.; Josse, F. *Analytical Chemistry.* **2007**, 79, 1646-1654.
4. J. Bouchaud, B. Knoblich, H. Wicht. *Proceedings of the 36th European Microwave Conference.* **2007**, 1076-1079.
5. S. Pourkamali, A. Hashimura, R. Abdolvand, G.K. Ho, A. Erbil, F. Ayazi. *Journal of Microelectromechanical Systems.* **2003**, 12, 487-496.
6. R. Abdolvand, F. Ayazi. *Journal of Microelectromechanical Systems.* **2006**, 15, 1139-1144.